ECOLOGY

Extensive marine anoxia during the terminal Ediacaran Period

Feifei Zhang[1]*, Shuhai Xiao[2], Brian Kendall[3], Stephen J. Romaniello[1], Huan Cui[4], Mike Meyer[5], Geoffrey J. Gilleaudeau[1], Alan J. Kaufman[6], Ariel D. Anbar[1,7]

The terminal Ediacaran Period witnessed the decline of the Ediacara biota (which may have included many stem-group animals). To test whether oceanic anoxia might have played a role in this evolutionary event, we measured U isotope compositions ($\delta^{238}U$) in sedimentary carbonates from the Dengying Formation of South China to obtain new constraints on the extent of global redox change during the terminal Ediacaran. We found the most negative carbonate $\delta^{238}U$ values yet reported (−0.95 per mil), which were reproduced in two widely spaced coeval sections spanning the terminal Ediacaran Period (551 to 541 million years ago). Mass balance modeling indicates an episode of extensive oceanic anoxia, during which anoxia covered >21% of the seafloor and most U entering the oceans was removed into sediments below anoxic waters. The results suggest that an expansion of oceanic anoxia and temporal-spatial redox heterogeneity, independent of other environmental and ecological factors, may have contributed to the decline of the Ediacara biota and may have also stimulated animal motility.

INTRODUCTION

Macroscopic and morphologically complex multicellular eukaryotes, including possible representatives of stem-group animal phyla, diversified in the second half of the Ediacaran Period starting ~570 million years (Ma) ago (*1*). The fossil record of these eukaryotes is sometimes referred to as the Ediacara biota (*2*). The Ediacara biota reached their maximum taxonomic and morphological diversity about 560 Ma ago, then subsequently declined in the terminal Ediacaran Period (~550 to 541 Ma ago), and almost completely disappeared at the Ediacaran-Cambrian transition about 541 Ma ago (*2*–*4*). The causes of the decline and eventual disappearance of the Ediacara biota remain a subject of intensive debate (*3*, *5*, *6*).

Changes in ocean redox conditions are often implicated as a driver of the decline of the Ediacara biota (*3*, *7*–*9*). Given the physiological requirements of many Ediacaran organisms, particularly macroscopic diffusion-dependent stem-group animals (*10*), O_2 availability is expected to have an impact on the distribution of the Ediacara biota both locally and globally (*11*–*14*). It has been shown that Ediacaran organisms were locally restricted to oxygenated environments under highly dynamic redox conditions (*13*). Planavsky *et al.* (*12*) suggested that generally low global O_2 availability until ~750 Ma ago was a key factor delaying the rise of multicellular animals. Canfield *et al.* (*11*) specifically linked the initial diversification of the Ediacara biota at ~570 Ma with a deep ocean oxygenation event (*15*, *16*). However, the possible relationship between ocean redox evolution and the decline of the Ediacara biota has not been clearly demonstrated.

Previous studies reported geochemical evidence for oceanic anoxia at the Ediacaran-Cambrian boundary (*7*, *8*). However, current fossil evidence points to a significant decline in biodiversity in the terminal Ediacaran Period, up to 10 Ma ago before the Ediacaran-Cambrian boundary (*3*, *5*). This temporal mismatch and a protracted decline of the biota have prompted some to favor a biotic replacement model as an explanation for the decline of the Ediacara biota (*3*, *5*). This model suggests that Ediacaran organisms were progressively replaced by newly evolved bilaterian animals, which may have directly or indirectly modulated the availability of resources, including both substrates and nutrients (*3*).

Resolving this debate requires the integration of paleontological and geochemical data. At a global scale, this integration is challenging because precise stratigraphic correlation of Ediacaran strata is difficult (*17*) and proxies for global ocean redox conditions are few. Sperling *et al.* (*18*) assembled a global compilation of Fe speciation data, but the temporal resolution of this compilation is dependent on interregional correlation and is insufficient for the reconstruction of short-term oceanic redox dynamics in the terminal Ediacaran Period. In contrast, other studies have focused on local redox proxies from fossiliferous successions so that geochemical and paleontological data were collected from the same successions, avoiding the challenges of interregional correlation. For example, Darroch *et al.* (*5*), Wood *et al.* (*13*), and Tostevin *et al.* (*6*) applied Fe speciation and Ce anomalies to carbonates and siliciclastic rocks of the Nama Group to understand factors controlling the distribution and decline of the Ediacara biota in the terminal Ediacaran Period. Darroch *et al.* (*5*) presented Fe speciation data from a single terminal Ediacaran section that records lower genus richness than older Ediacaran assemblages. Their data show that these sediments that record declining diversity of the Ediacara biota were deposited in oxic environments, and they concluded that oxygen stress probably did not play a role in the decline of the Ediacara biota. However, their data are also consistent with the possibility that terminal Ediacaran organisms were challenged by a global expansion of anoxia and were restricted to oxic refugia in oceans with highly heterogeneous redox conditions. Wood *et al.* (*13*) and Tostevin *et al.* (*6*) have shown that terminal Ediacaran organisms are not found in anoxic environments and that their distribution is strongly controlled by oxygen availability. Terminal Ediacaran organisms may have been globally challenged by an expansion of oceanic anoxia and locally relegated to oxic refugia.

Uranium isotopes ($^{238}U/^{235}U$, denoted as $\delta^{238}U$) in carbonates may be uniquely suited to differentiate global from local perturbations

[1]School of Earth and Space Exploration, Arizona State University, Tempe, AZ 85287, USA. [2]Department of Geosciences, Virginia Tech, Blacksburg, VA 24061, USA. [3]Department of Earth and Environmental Sciences, University of Waterloo, Waterloo, Ontario N2L 3G1, Canada. [4]Department of Geoscience and NASA Astrobiology Institute, University of Wisconsin-Madison, Madison, WI 53706, USA. [5]Carnegie Institution for Science, Washington, DC 20005, USA. [6]Geology Department and Earth System Science Interdisciplinary Center, University of Maryland, College Park, MD 20742, USA. [7]School of Molecular Sciences, Arizona State University, Tempe, AZ 85287, USA.
*Corresponding author. Email: fzhang48@asu.edu

in ocean redox chemistry (*19*–*21*) and therefore to test the degree to which changing global ocean redox conditions may have shaped the evolutionary trajectory of the Ediacara biota. To meet this challenge and to specifically address the question of whether the decline of the Ediacara biota was driven by an episode of expanded marine anoxia, we analyzed $\delta^{238}U$ in carbonates from the Dengying Formation (South China; ca. 551 to 541 Ma ago) that also contains terminal Ediacaran macrofossils characteristic of the Nama assemblage. The integration of $\delta^{238}U$ data and paleontological data from the same suite of rocks allows us to reconstruct global ocean redox conditions at a time when the Ediacara biota began to decline.

THE URANIUM ISOTOPE PROXY

Variations in global ocean $\delta^{238}U$ may reflect changes in the global ocean redox state because the extent to which seawater U isotopes are fractionated from riverine input is sensitive to the extent of ocean anoxia (see the Supplementary Materials for inputs and outputs of uranium in the ocean).

Uranium has a long ocean residence time [~5×10^5 years; (*22*)] relative to the time scale of ocean mixing (~10^3 years). Hence, $\delta^{238}U$ is uniform within and between different modern ocean basins (*23*, *24*) and will tend to be well mixed (except in highly restricted marine basins) even when the extent of ocean oxygenation is significantly lower than today (*21*). Uranium occurs in two redox states in natural waters: soluble U(VI) under oxygenated conditions and insoluble U(IV) under anoxic conditions. Isotope fractionation between U(IV) and U(VI) is driven by the dominance of nuclear volume effects (*25*). As a result, during reduction of U(VI) to U(IV), the reduced U(IV) is enriched in the heavier ^{238}U isotope, leaving the remaining dissolved U(VI) reservoir depleted in ^{238}U. Microbially mediated reduction of U(VI) to U(IV) under anoxic conditions at the sediment-water interface results in a large and detectable change in $^{238}U/^{235}U$ (*26*, *27*). Because ^{238}U is preferentially reduced and immobilized relative to ^{235}U, the $\delta^{238}U$ of global seawater U(VI) decreases as the areal extent of bottom water anoxia increases (*19*–*21*).

The sensitivity of seawater $\delta^{238}U$ to perturbations in global ocean redox conditions makes U isotopes a promising tool to identify time intervals of expanded ocean anoxia or rapid ocean oxygenation (*19*–*21*, *28*). Assuming steady state, the implied changes to the extent of U removal into anoxic/euxinic sediments can be described by a mass balance equation for the fraction of anoxic/euxinic sinks and their isotopic composition, respectively (see the Supplementary Materials for U isotope mass balance in the ocean)

$$\delta^{238}U_{input} = (f_{anoxic} \times \delta^{238}U_{anoxic}) + (f_{other} \times \delta^{238}U_{other}) \quad (1)$$

$$\delta^{238}U_{anoxic} = \delta^{238}U_{seawater} + \Delta_{anoxic} \quad (2)$$

$$\delta^{238}U_{other} = \delta^{238}U_{seawater} + \Delta_{other} \quad (3)$$

where the subscripts seawater, input, anoxic, and other denote the seawater, riverine input, anoxic/euxinic sink, and all other sedimentary sinks, respectively. f_{anoxic} and f_{other} represent the fraction of total U removed to each sediment type, and Δ_{anoxic} and Δ_{other} represent the isotope fractionation factor between seawater and each sediment type. In this simplified calculation, all types of sinks other than anoxic/euxinic sinks are lumped into a single "other" sink (see the Supplementary Materials for other sinks and Δ_{other}). Because the fraction of U removed into anoxic/euxinic sedimentary sinks is intimately coupled to the proportion of anoxic/euxinic versus oxic bottom waters, $\delta^{238}U_{seawater}$ can be used to calculate the area of anoxic/euxinic seafloor using Eq. 4, derived from the U isotope mass balance and assuming a first-order relationship between U burial rate into each sink and the global seawater U reservoir (see the Supplementary Materials for detailed calculation and parameters used in the calculation)

$$\delta^{238}U_{seawater} = \delta^{238}U_{input} - \frac{A_{anoxic} \cdot k_{anoxic} \cdot \Delta_{anoxic} + A_{suboxic} \cdot k_{suboxic} \cdot \Delta_{suboxic} + A_{oxic} \cdot k_{oxic} \cdot \Delta_{oxic}}{A_{anoxic} \cdot k_{anoxic} + A_{suboxic} \cdot k_{suboxic} + A_{oxic} \cdot k_{oxic}} \quad (4)$$

where A_{anoxic}, $A_{suboxic}$, and A_{oxic} denote anoxic/euxinic seafloor area, suboxic seafloor area, and oxic seafloor area ($A_{anoxic} + A_{suboxic} + A_{oxic} = A_{ocean}$, where A_{ocean} is the seafloor area of the whole ocean), respectively, and k_{anoxic}, $k_{suboxic}$, and k_{oxic} represent removal rate constants for each sink type.

On the basis of mass balance modeling of the marine U isotope budget, seawater is expected to have lower $\delta^{238}U$ at times of expanded ocean anoxia and higher $\delta^{238}U$ at times of extensive ocean oxygenation. These variations in seawater $\delta^{238}U$ can potentially be recorded in the sedimentary record, specifically by marine carbonate rocks (*19*–*21*, *23*, *28*, *29*). Studies on the modern Bahamian carbonate platform suggest that primary biogenic carbonates (for example, scleractinian corals, calcareous green and red algae, ooids, and mollusks) are capable of faithfully recording seawater $\delta^{238}U$ since minor $^{238}U/^{235}U$ fractionation occurs during coprecipitation with carbonate minerals (*29*). However, the $\delta^{238}U$ of sedimentary carbonates may be isotopically heavier than seawater by 0.2 to 0.4 per mil (‰) in cases of pore water anoxia during early diagenesis (*29*). After properly screening for sample diagenesis (discussed in detail below and see also the Supplementary Materials), variations of $\delta^{238}U$ in ancient marine carbonates can be used to reconstruct secular variation in global ocean redox conditions (*19*–*21*, *28*, *29*).

GEOLOGICAL BACKGROUND

The Ediacaran System in South China is represented by the Doushantuo Formation (~635 to 551 Ma) and the Dengying Formation (551 to 541 Ma), which are overlain by the lower Cambrian Yanjiahe Formation and its equivalents. We sampled the terminal Ediacaran Dengying Formation at the Wuhe section in the Yangtze Gorges area and at the Gaojiashan section in southern Shaanxi Province (Fig. 1). The age constraints of the Dengying Formation come from a 551-Ma U-Pb zircon date in the underlying Doushantuo Formation (*30*) and an estimated 541-Ma age for the Ediacaran-Cambrian boundary (*9*). Paleogeographically, these two sections were located on carbonate platforms on the southeastern and northwestern margins of the Yangtze Block (*31*–*33*). At Wuhe, the Dengying Formation includes the basal Hamajing Member (peritidal dolostone), the middle Shibantan Member (subtidal limestone), and the upper Baimatuo Member (peritidal dolostone). These three members are lithostratigraphically similar to, and traditionally correlated with, the Algal Dolomite, Gaojiashan, and Beiwan members

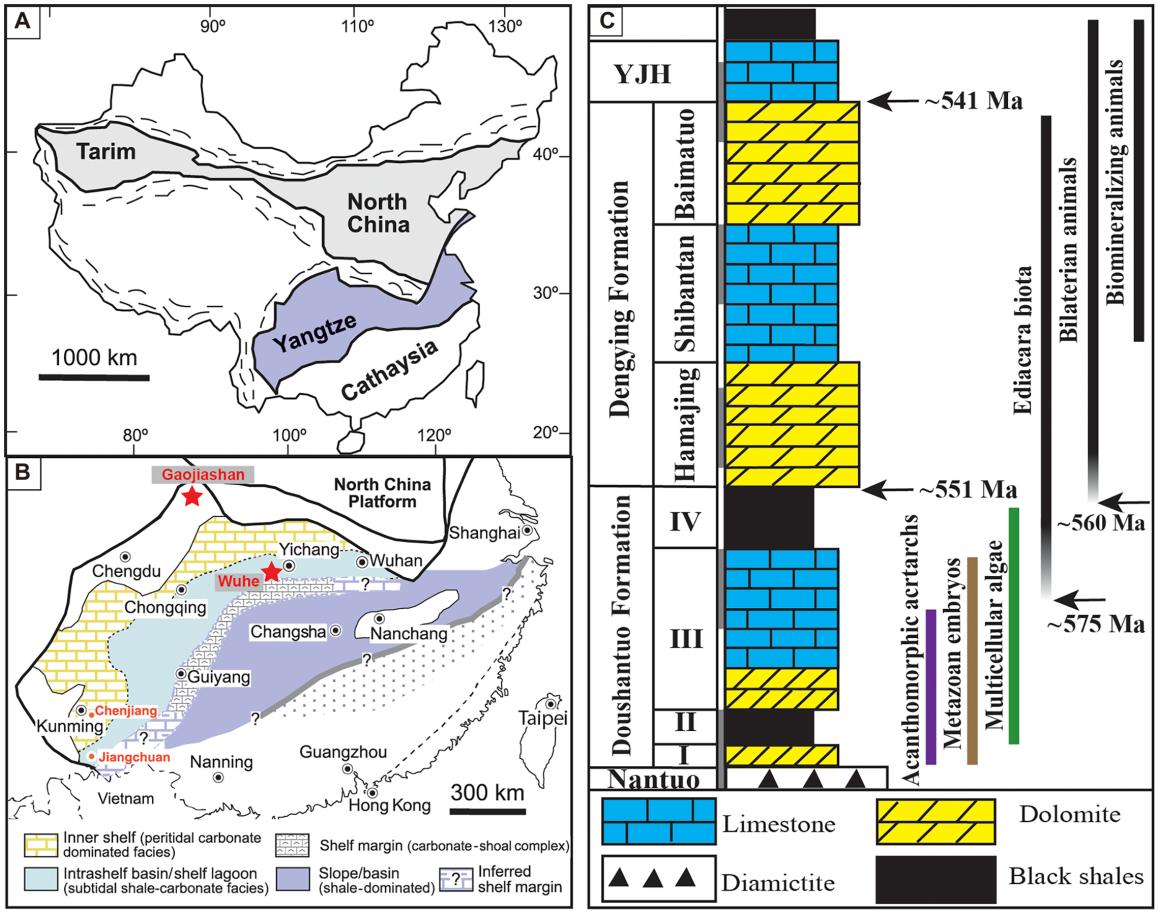

Fig. 1. Reconstructed Ediacaran depositional environments on the Yangtze Craton with the location of the study sections and integrated lithostratigraphy and biostratigraphy of the terminal Ediacaran Dengying Formation, South China. (**A**) Simplified map showing the location of the Yangtze Block (*31*, *32*). (**B**) Paleogeographic map of the Yangtze Block showing the location of the Wuhe section and the Gaojiashan section. (**C**) Simplified stratigraphic column of the Ediacaran Doushantuo and Dengying formations and the Early Cambrian Yanjiahe Formation (YJH), as well as the chronology for the evolution of major Ediacaran animal groups (*15*).

at Gaojiashan (*33*). The Shibantan and Gaojiashan members in South China may be partially correlated with the upper Nafun Group–lower Ara Group in Oman, the upper Zaris Formation–Urusis Formation of the Nama Group in Namibia, and the Khatyspyt Formation in Arctic Siberia, on the basis of chemostratigraphic data and the occurrence of the earliest skeletal animal fossils such as *Cloudina* (*17*).

We analyzed 27 samples from the Gaojiashan Member at the Gaojiashan section, 56 samples from the Dengying Formation at the Wuhe section, and 6 samples of the Early Cambrian Yanjiahe Formation at the Wuhe section in this study. Detailed geological background of the study sites and analytical methods have been summarized in the Supplementary Materials.

RESULTS

We observed large stratigraphic variations in $\delta^{238}U$ in the studied sections (Fig. 2 and fig. S2). At Wuhe, the $\delta^{238}U$ of the Hamajing Member declines upsection from −0.45 to −1.19‰. The Shibantan Member has a relatively narrow variation in $\delta^{238}U$ from −0.81 to −1.20‰, with an average of −0.97 ± 0.18‰. In the Baimatuo Member, a positive excursion in $\delta^{238}U$ from −0.95 to −0.50‰ occurs at the Precambrian-Cambrian boundary. This positive shift in $\delta^{238}U$ is followed by a negative excursion in $\delta^{238}U$ from −0.52 to −0.82‰ in the overlying Yanjiahe Formation.

At Gaojiashan, $\delta^{238}U$ in the lower Gaojiashan Member varies between −0.18 and −0.76‰ (fig. S2; only data that passed the diagenetic evaluation described below are shown in Fig. 2). The $\delta^{238}U$ of the middle-upper Gaojiashan Member shows relatively narrow variations in $\delta^{238}U$ from −0.80 to −1.17‰, with an average of −0.94 ± 0.20‰; these values are indistinguishable from those of the stratigraphically equivalent Shibantan Member.

EVIDENCE FOR PRIMARY OCEANOGRAPHIC SIGNALS

Previous studies cited low Sr content, high Mn content, high Mn/Sr ratio, and ^{18}O depletion as characteristics of diagenetic alteration by meteoric or burial fluids (*34*, *35*). Here, we adopted a conservative Mn/Sr ratio of ≤2.5 as an initial diagenetic alteration threshold. The majority of limestone and dolostone samples from the Hamajing, Gaojiashan, Shibantan, Baimatuo, and Yanjiahe members have Mn/Sr ratios less than 2.5 and are thus regarded as least-altered samples with the potential to preserve primary geochemical signatures. In addition, we also investigated the correlations of $\delta^{238}U$-Mn content, $\delta^{238}U$-Sr content, $\delta^{238}U$-Mn/Sr, $\delta^{238}U$-Sr/(Mg + Ca), $\delta^{238}U$-Mn/(Mg + Ca), and $\delta^{238}U$-$\delta^{18}O$ for samples

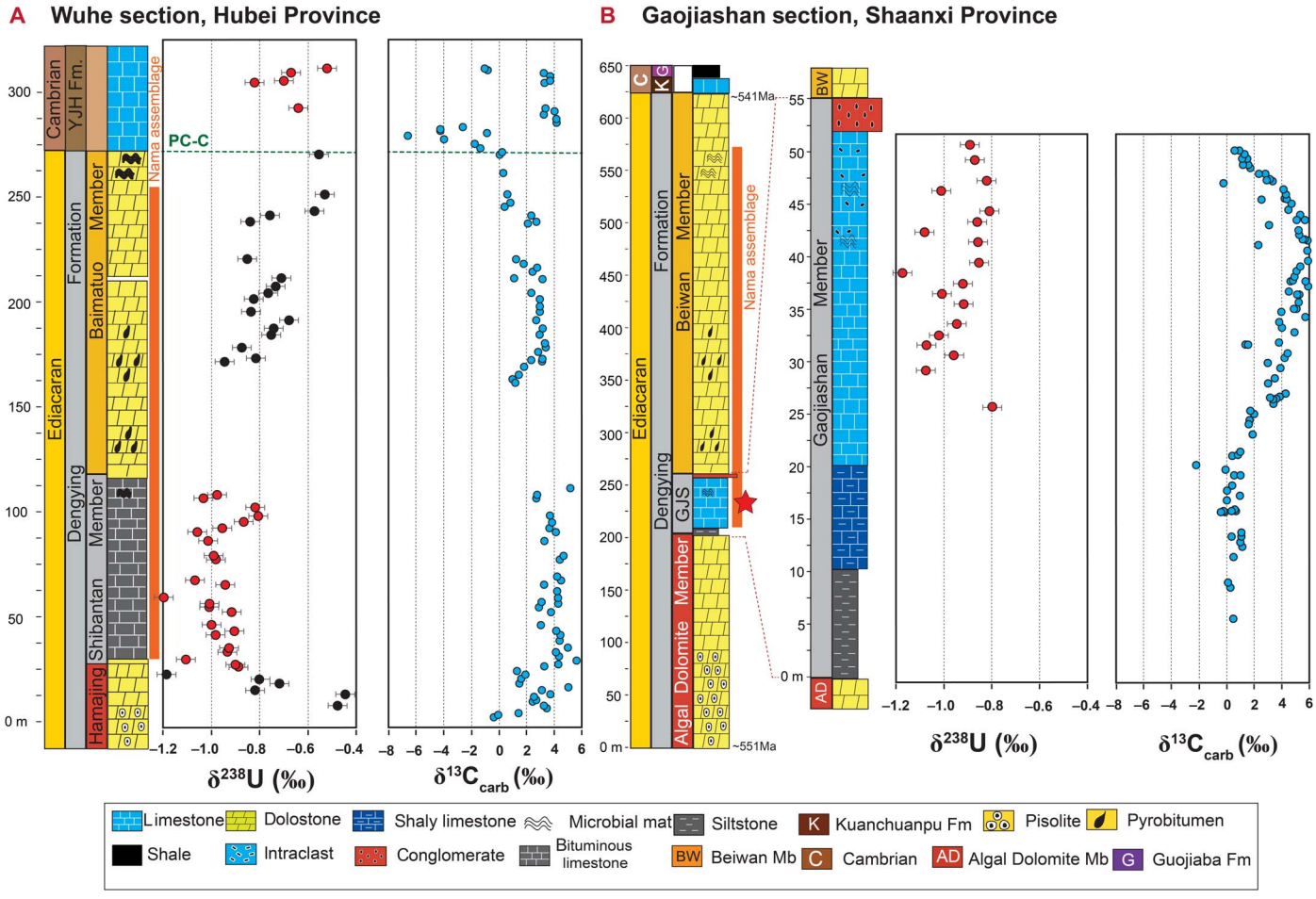

Fig. 2. Geochemical profiles of the terminal Ediacaran Dengying Formation at the Wuhe and Gaojiashan sections. Stratigraphic columns and $\delta^{13}C$ data of Gaojiashan (GJS) are from Cui *et al.* (*31*). $\delta^{238}U$ data from the Hamajing Member and samples with Mn/Sr > 2.5, Rb/Sr > 0.02, and Al > 0.35% are excluded in this plot, but they are shown in fig. S2. PC-C denotes Precambrian-Cambrian boundary. Red and black circles represent data from limestone samples and from dolostone samples, respectively.

with Mn/Sr ratios less than 2.5 (table S2). No systematic trends are apparent, suggesting that interaction with meteoric or burial fluids did not significantly alter $\delta^{238}U$ (see the Supplementary Materials for a more in-depth discussion of diagenesis).

In carbonates that underwent extensive recrystallization, $\delta^{238}U$ may be diagenetically altered, and therefore, petrographic studies and comparison of data from multiple coeval sections are necessary to confirm that carbonate $\delta^{238}U$ captures depositional conditions (*36*). The Gaojiashan, Shibantan, and Yanjiahe members typically preserve pristine sedimentary fabrics such as microbially laminated micrites (see the Supplementary Materials for details) and $\delta^{13}C$ signatures consistent with marine carbonates of similar age (*31*, *33*, *35*), suggesting that their geochemistry was not strongly altered by diagenesis. These petrographic observations and similar $\delta^{238}U$ signatures in two widely separated limestone sections together strongly suggest that $\delta^{238}U$ was not significantly altered by diagenesis. The Hamajing and Beiwan members are characterized by micritic to microsparitic fabric-retentive dolomite, with no apparent evidence for fabric-destructive dolomitization (*35*) (see the Supplementary Materials for details). The majority of dolostone samples (27 of 30) from the Hamajing and Beiwan members have $\delta^{18}O$ values greater than −6‰, and $^{87}Sr/^{86}Sr$ values from both the Hamajing (0.7085 to 0.7088) and Baimatuo (0.7087 to 0.7102) members are well within the range of typical latest Ediacaran seawater (0.7085 to 0.7100) (*34*, *35*, *37*). A simple model of carbonate diagenesis predicts that U is more robust than $\delta^{18}O$ and $^{87}Sr/^{86}Sr$ with respect to diagenetic alteration (*20*). Therefore, these latest Ediacaran carbonates appear capable of preserving the $\delta^{238}U$ of contemporaneous seawater.

Changes in lithology—such as dolomitization—could also potentially affect $\delta^{238}U$, but this is unlikely to be a major factor in the sections studied here. Romaniello *et al.* (*29*) reported a sharp decrease in $\delta^{238}U$ below −0.6‰ corresponding to the appearance of dolomite in a tidal pond in the Bahamian carbonate platform. Although the cause for these negative values is not yet fully understood, $\delta^{238}U$ is strongly correlated with the Mg/Ca molar ratio ($R^2 = 0.96$), a proxy that indicates the extent of dolomitization. By contrast, although the Shibantan Member and the Yanjiahe Formation are composed of limestone and the Hamajing Member and the Baimatuo Member are composed of dolostone, no statistically significant correlations are observed between $\delta^{238}U$ and Mg/Ca molar ratio for these carbonates at Wuhe ($R^2 = 0.22$). Furthermore, a recent global compilation of $\delta^{238}U$ variation across the Permian-Triassic boundary indicates that both the dolomitized sections and the nondolomitized sections show congruent $\delta^{238}U$ records, indicating that dolomitization alone may not significantly alter paleo-$\delta^{238}U$

records (*21*). These observations suggest that dolomitization has not systematically altered the primary U isotopic record in the Wuhe section (see the Supplementary Materials for details).

The effect of other changes in mineralogy—such as transformation of aragonite to calcite—on $\delta^{238}U$ is also likely to be small or negligible. The Shibantan and Gaojiashan limestone (low-Mg calcite) was likely originally aragonite and/or high-Mg calcite. Prior studies have shown that the distribution coefficient of U into aragonite is higher than that for calcite (*38*). In contrast, the effect of mineralogy and carbonate ion concentration on $\delta^{238}U$ is more limited. Uranium isotope measurements of aragonite and high-Mg calcite primary precipitates exhibit no offset from seawater (*29*). Laboratory-precipitated calcite and aragonite at pH ~8.5 showed only minor (<0.13‰) U isotope fractionation between the liquid medium and the solid (*39*). In contrast, at pH ~7.5, the precipitates of both polymorphs exhibit no U isotope fractionation (*39*). Therefore, changing carbonate mineralogy can result in large differences in uranium concentrations but only small changes in the isotopic composition (*20*).

Detrital U contamination could also cause a $\delta^{238}U$ offset. Our samples were dissolved in 1 M hydrochloric acid (HCl) before extraction of U, which will minimize dissolution of any noncarbonate minerals (for example, silicates) and organic matter. This expectation is supported by the high U/Al ratios in our analyses. The U/Al ratios of our dissolved samples are two orders of magnitude higher than the upper continental crust ratio [~0.331 parts per million (ppm)/weight % (wt %); see the Supplementary Materials for details]. Assuming that all the measured Al comes from detrital material, and using a U/Al ratio of 0.331 (ppm/wt %) for the upper continental crust, we estimate that detrital U accounts for <2% of total U in the dissolved samples from Wuhe and <10% of total U for the majority of Gaojiashan samples. Although the estimated amount of U derived from detrital material is different between the Shibantan Member at Wuhe and its equivalent Gaojiashan Member at Gaojiashan, the $\delta^{238}U$ signals of these two members are essentially identical. Furthermore, there is no correlation between $\delta^{238}U$ and Al contents ($R^2 = 0.19$, $P = 0.38$ for Shibantan carbonates; $R^2 = 0.11$, $P = 0.67$ for Gaojiashan carbonates). Therefore, we are confident that our observed $\delta^{238}U$ trends are not related to detrital contamination.

Changes in redox conditions of the local water column might affect the ability of carbonate sediments to passively incorporate U(VI), which is essential for capturing the $\delta^{238}U$ value of seawater (*29*). Specifically, it is essential that carbonates act as an oxic sink for U, with no change in redox state (and thus a potential isotope fractionation) of U in the local water column. We examined water column redox conditions by looking at the Ce anomaly (Ce/Ce*) in our carbonates. The Ce anomalies at Wuhe and at Gaojiashan range between 0.29 and 0.79 (mean of 0.50) and between 0.70 and 0.98 (mean of 0.74), respectively, suggesting that local water column redox conditions at Wuhe and at Gaojiashan were oxic (*40*). This finding confirms that our carbonates can be considered an oxic sink for U and thus can passively capture the $\delta^{238}U$ signal of seawater.

In addition to the water column, it is also important to consider pore water redox conditions because they can also affect the ability of carbonate sediments to preserve the $\delta^{238}U$ value of seawater. For example, under sulfidic pore water conditions, bulk carbonate sediments may incorporate ^{238}U-enriched U(IV), leading to a $\delta^{238}U$ value that is 0.2 to 0.4‰ heavier than seawater. We examined this possibility using Mo concentrations and correlations between $\delta^{238}U$ and U/(Mg + Ca) and Mo/(Mg + Ca) ratios. Under sulfidic pore water conditions, U and Mo become authigenically enriched in carbonate (*29*), thus increasing U/(Mg + Ca) and Mo/(Mg + Ca) values. In our samples, Mo concentrations are significantly lower than those in modern Bahamas box core sediments by approximately two orders of magnitude, and there is no systematic stratigraphic variation in U/(Mg + Ca) or Mo/(Mg + Ca) ratios, indicating that pore water euxinia during early diagenesis was less prevalent than that on the modern Bahamian carbonate platform (*29*). Furthermore, there are no statistically significant correlations between $\delta^{238}U$ and U/(Mg + Ca) and Mo/(Mg + Ca) in our carbonates (table S2). Thus, the $\delta^{238}U$ record in these latest Ediacaran carbonates was likely not significantly altered by pore water anoxia (see the Supplementary Materials for details). We also note that if our carbonates were influenced by pore water anoxia, then our estimation of terminal Ediacaran seawater $\delta^{238}U$ can be considered conservative, such that we would underestimate the extent of ocean anoxia in the terminal Ediacaran ocean.

After consideration of each of these factors, we conclude that the Dengying carbonates likely reflect the $\delta^{238}U$ of late Ediacaran seawater. Samples that pass our diagenetic and detrital quality control checks are plotted in Fig. 2.

The Shibantan Member and the stratigraphically correlated Gaojiashan Member yield the most negative carbonate $\delta^{238}U$ values ever reported from the geological record. The average $\delta^{238}U$ values of the Shibantan Member and the Gaojiashan Member are −0.97 ± 0.18‰ and −0.95 ± 0.21‰, respectively. The Hamajing Member, Baimatuo Member, and Yanjiahe Formation yield higher $\delta^{238}U$ values of −0.74 ± 0.54‰, −0.72 ± 0.25‰, and −0.71 ± 0.16‰, respectively (Fig. 2). The extremely negative $\delta^{238}U$ values in the Gaojiashan and Shibantan members are associated with positive carbonate carbon isotope excursions in both sections (Fig. 2). A positive shift in $\delta^{238}U$, starting in the Baimatuo Member and peaking at the Dengying-Yanjiahe boundary (maximum values of −0.6 to −0.5‰), occurs coevally with a negative carbonate carbon isotope excursion (Fig. 2 and fig. S1) that has been observed globally near the Ediacaran-Cambrian boundary (*8*, *9*, *17*). This positive $\delta^{238}U$ excursion is followed by another shift back to relatively negative $\delta^{238}U$ values (minimum values of −0.7 to −0.8‰) above the Ediacaran-Cambrian boundary, although more data from Cambrian age sediments are required to confirm this pattern.

EXTENSIVE OCEANIC ANOXIA IN THE LATEST EDIACARAN OCEAN

Since diagenesis cannot easily explain the very negative $\delta^{238}U$ values observed in the Shibantan/Gaojiashan members, the data likely indicate an episode of extensive expansion in marine anoxia. We evaluate the extent and the possible causes for those extremely negative values below.

First, we evaluate the extent of oceanic anoxia based on U isotope mass balance equations (Eqs. 1 to 3) for the terminal Ediacaran oceans (see the Supplementary Materials for uranium isotope mass balance constraints on U removal to anoxic sediments). We use the following values for terminal Ediacaran seawater: $\delta^{238}U_{seawater} = -0.95‰$ (average isotopic composition of the Shibantan and Gaojiashan members), $\delta^{238}U_{input} = -0.34‰$, $\delta^{238}U_{anoxic} = -0.95‰ + \Delta_{anoxic}$, and $\delta^{238}U_{other} = -0.91‰$ (that is, $-0.95‰ + \Delta_{other}$, assuming a constant Δ_{other} of 0.04‰). Using a Δ_{anoxic} of 0.6‰, which is a representative average observed in the modern Saanich Inlet (*41*), we calculate that $f_{anoxic} \approx 1$, meaning that anoxic/euxinic sinks were responsible for nearly 100% of the U removal to sediments when the Shibantan/Gaojiashan members were deposited (Fig. 3A). A simple mass balance seafloor area calculation

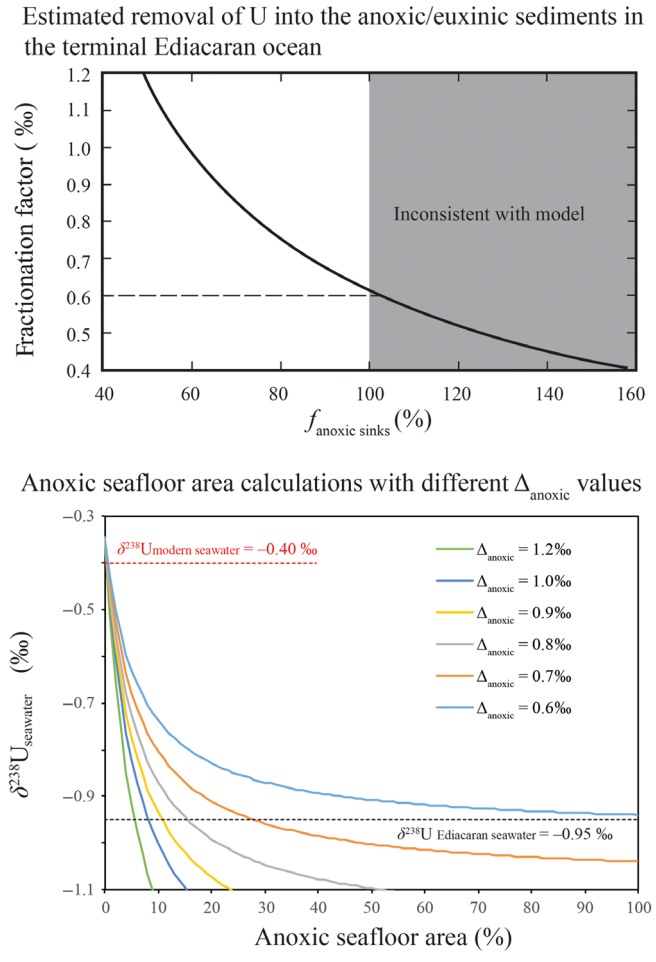

Fig. 3. Model results. (**A**) The fraction of oceanic U inputs removed into anoxic/euxinic sediments (horizontal axis) varies as a function of the fractionation factor (Δ_{anoxic}; vertical axis) between seawater and anoxic/euxinic sediments. The estimates are based on calculations using the average carbonate $\delta^{238}U$ of the Shibantan/Gaojiashan members ($\delta^{238}U$ = –0.95‰). (**B**) Mass balance calculations show variations of seawater $\delta^{238}U$ values as a function of anoxic seafloor area, keeping suboxic seafloor area fixed at 0% of total seafloor area and testing the sensitivity to possible Δ_{anoxic} values. In reality, suboxic seafloor area would co-vary with anoxic/euxinic seafloor area; thus, this modeling exercise gives us the lowest estimation of anoxic/euxinic seafloor area.

(Eq. 4) predicts that nearly ~100% of the seafloor area was covered by anoxic/euxinic sediments (Fig. 3B and see the Supplementary Materials for anoxic seafloor modeling area calculation). Hence, the data suggest that an episode of extensive ocean anoxia occurred during the terminal Ediacaran Period. However, this extreme scenario is inconsistent with the presence of benthic oxygen-breathing organisms in the terminal Ediacaran Period, necessitating a sensitivity test of the mass balance calculation to assess the impact of Δ_{anoxic} values on the model estimates.

The inferred extent of ocean anoxia calculated from the mass balance model depends on the average fractionation factor between seawater and anoxic/euxinic sediments. This parameter is not tightly constrained because data exist for only a small number of modern anoxic environments. Considering this uncertainty, we explored the effect of a large range of Δ_{anoxic} values (0.4 to 1.3‰) on the marine U isotope mass balance. The results are summarized in Fig. 3B. Large U isotope fractionations of between 0.68 and 0.99‰ have been reported during reduction of U(VI) to U(IV) by different species of metal-reducing bacteria (*26*, *27*). While studies of U reduction in modern anoxic marine basins commonly find apparent fractionation factors of Δ_{anoxic} = 0.6 ± 0.1‰ (*24*, *41*, *42*), these fractionation factors are interpreted to reflect diffusion-limited U reduction below the sediment-water interface, which reduces the magnitude of the apparent isotope fractionation factor by ~50% (*24*). Studies of U reduction in most modern anoxic basins have shown that little, if any, U reduction occurs directly in the water column (*41*, *42*). Nevertheless, there is some evidence that microbial U reduction can occur at significant rates directly in the water column of strongly reducing marine basins, such as Framvaren Fjord (*43*). Under these conditions, U reduction appears to be accompanied by a larger isotope fractionation factor of 1.0 to 1.3‰, similar to that predicted by laboratory experiments and theoretical calculations (*44*, *45*). Together, existing observations imply that reductive removal of U from seawater could result in effective isotope fractionation factors of 0.4 to 1.3‰ between euxinic sediments and the overlying water column. In contrast, the isotope fractionation of U isotopes under ferruginous conditions remains poorly known. A recent study suggested that U isotope fractionation may be similar in euxinic and ferruginous settings (*46*); however, another study has suggested that the fractionation of U isotopes under ferruginous conditions may be close to 0‰ (*36*). Further studies are needed to confirm the fractionation factor for ferruginous environments. We explore the implications of these uncertainties below.

Although the fraction of U removal into anoxic/euxinic sediments (Fig. 3A) and the calculated anoxic/euxinic seafloor areas (Fig. 3B) are very sensitive to Δ_{anoxic} values, extensive ocean anoxia is implicated for all plausible Δ_{anoxic} to drive terminal Ediacaran seawater $\delta^{238}U$ values as low as –0.95‰. For instance, when applying Δ_{anoxic} of 0.6, 0.8, 1.0, and 1.2‰, the calculated percentages of U removal into anoxic/euxinic sediments are 100, 75, 60, and 50%, respectively, and the estimated anoxic/euxinic seafloor areas are ~100, ~27, ~10, and ~6%, respectively. If we assume that the maximum value of Δ_{anoxic} likely to represent Neoproterozoic oceans is similar to the maximum Δ_{anoxic} values observed both in the modern Saanich Inlet (0.79‰) (*41*) and in the Black Sea (0.83‰) (*23*, *42*), then we calculate that f_{anoxic} = 0.7. This means that a minimum of 70% of the global riverine U input was removed into anoxic/euxinic organic-rich sediments when the Shibantan/Gaojiashan members were deposited. On the basis of this estimate and Eq. 4, our best estimate for the minimum global anoxic/euxinic seafloor area during the terminal Ediacaran is ~21%. Hence, a significant portion of the seafloor area (21 to 100%) overlain by anoxic/euxinic sediments during the terminal Ediacaran Period is indicated for all plausible fractionation factors between anoxic/euxinic sediments and seawater.

Our study highlights that marine anoxia may have been a global phenomenon from ca. 551 to 541 Ma, although there were likely redox fluctuations within local continental margin basins. For example, Fe-S-C systematics and redox-sensitive metal enrichments from latest Ediacaran sediments in South China suggest predominance of anoxia in deep-water settings (*14*, *47*, *48*), with oxic water masses only present in very shallow settings (*31*, *40*). The Fe speciation and Ce anomaly data from the Nama Group in Namibia suggest locally dynamic redox conditions with frequent anoxia in deepwater settings (*6*, *7*, *13*). The Fe speciation data from Newfoundland in Canada suggest locally oxic redox conditions (*11*).

A gradual recovery to heavier U isotope values occurs in the stratigraphically overlying Baimatuo Member, with the highest $\delta^{238}U$ values (–0.6 to –0.5‰) occurring at the Ediacaran-Cambrian boundary

(Fig. 2). Above the boundary, $\delta^{238}U$ data hint at a return to low values (−0.7 to −0.8‰), although more data are needed to confirm this pattern. These observations suggest a temporary transition to more oxygenated conditions at the Ediacaran-Cambrian boundary (*14*, *49*), followed by a return to extensive ocean anoxia in the earliest Cambrian (*14*, *48*).

Because the U isotope fractionation under ferruginous conditions is poorly constrained, it is possible that the fluctuating $\delta^{238}U$ values in the Dengying Formation represent global redox oscillation between ferruginous and euxinic conditions, rather than oscillation between oxic and anoxic conditions. For example, if the fractionation factor associated with U removal to ferruginous sediments is close to 0‰ [as has been suggested by Hood *et al.* (*36*)], then the positive $\delta^{238}U$ shift observed in the upper Wuhe section could be explained by a shift from dominantly euxinic to ferruginous conditions. However, it is more likely that the variations reflect a shift between anoxic and oxic conditions because higher $\delta^{238}U$ values in the lowest Hamajing and upper Baimatuo members and in the lowest Yanjiahe Formation (Fig. 2) are consistent with existing evidence for widespread ocean oxygenation immediately preceding the Hamajing stage (*50*) and at the Ediacaran-Cambrian boundary (*14*, *49*). Regardless, the main conclusion still holds that the terminal Ediacaran Period experienced extensive ocean anoxia (euxinic or ferruginous), although the detailed redox history of this time period will not be resolved until the U isotope fractionation in ferruginous settings is better understood.

The causes of rapid (million-year time scale) variations in global marine redox chemistry during the terminal Ediacaran Period are unclear and merit further study. However, variations between oxic and anoxic conditions may have been linked to changes in continental weathering fluxes and increased marine PO_4^{3-} levels. Phosphorus is commonly considered to be the ultimate biolimiting nutrient on geological time scales, and it plays a role in controlling the amount and spatial distribution of dissolved O_2 in the oceans (*51*). The terminal Ediacaran Period was associated with high continental weathering as indicated by the significant rise in seawater $^{87}Sr/^{86}Sr$ (*34*, *35*, *37*). High continental weathering rates could have increased marine phosphorus levels, thus stimulating marine productivity. On a short time scale (10^4 years), increased phosphorus input to the ocean would have led to rapid increases in primary production, higher O_2 demand, and deepwater anoxia and lower seawater $\delta^{238}U$ values (for example, the Shibantan/Gaojiashan stage and the early Baimatuo stage) (*51*). On a long time scale (10^6 years), it would have tended to increase organic carbon burial and atmospheric oxygen (*51*) and elevated marine sulfate concentrations (*16*, *31*), ocean oxygenation, extensive phosphorite formation (*49*), and higher seawater $\delta^{238}U$ values in the latest Ediacaran and earliest Cambrian ocean (for example, the late Baimatuo stage and the earliest Yanjiahe stage).

DYNAMIC OCEAN REDOX CONDITIONS AT THE EDIACARAN-CAMBRIAN TRANSITION

The geochemical data from this study combined with previous Ediacaran and Early Cambrian paleoredox studies yield a complex picture of oscillatory ocean redox conditions at the Ediacaran-Cambrian transition (Fig. 4). Fe-S-C systematics and redox-sensitive metal enrichments in organic-rich mudrocks (~635 to ~551 Ma) revealed three distinctive Ediacaran ocean oxygenation events at ca. 635, ca. 580, and ca. 560 Ma ago, with ocean anoxia possibly dominating the intervals between these oxygenation events (*14*, *52*). Studies focusing on the Shuram/Wonoka negative carbon isotope excursion (~580 to ~553 Ma, although the time and duration of this event are still uncertain) provided evidence of profound deep ocean oxygenation (*15*, *16*), although other studies argued that the global response of ocean redox chemistry at this time was likely complex (*14*, *18*, *47*). Organic-rich mudrocks deposited near the end of the Shuram/Wonoka excursion have high Mo enrichments and isotopically heavy U and Mo isotope compositions that point to an episode of extensive ocean oxygenation ca. 560 to 551 Ma ago (*14*, *50*, *52*). Here, we provide strong evidence for an episode of extensive ocean anoxia that follows this episode of oxygenation. Geochemical studies focusing on the Ediacaran-Cambrian boundary (~541 Ma) and the earliest Cambrian also present a complex picture of ocean redox chemistry, with apparently conflicting views of both oxygenation (*14*, *49*) and anoxia (*7*, *8*). However, our new $\delta^{238}U$ data provide evidence of an increase in global ocean oxygenation at the Ediacaran-Cambrian boundary, consistent with prior redox-sensitive trace metal enrichment and Mo isotope evidence of ocean oxygenation at the Ediacaran-Cambrian boundary (*14*, *49*). Therefore, the overall picture emerging from this study and prior studies is that global marine redox evolution across the Ediacaran-Cambrian transition was not a simple unidirectional march toward oxygenation but a dynamic and more complicated history than expected, with rapid oscillations between anoxic and oxic conditions.

OCEAN ANOXIA AND THE DECLINE OF THE EDIACARA BIOTA

Although the geochronological constraints on Ediacaran successions are generally poor, available data seem to suggest that the Ediacara biota consists of three taxonomically distinct assemblages that at least partially represent evolutionary successions (*2*): the Avalon (~570 to 560 Ma ago), White Sea (~560 to 550 Ma ago), and Nama (~550 to 540 Ma ago) assemblages. The Shibantan Member of the Dengying Formation (~551 to 541 Ma ago) studied in this paper contains *Cloudina* that is only found in the Nama assemblage (*33*) and taxa (for example, *Rangea* and *Pteridinium*) that are commonly present in the Nama Group (*53*) but does not yield any fossils (for example, *Dickinsonia* and *Yorgia*) that are characteristic of the White Sea assemblage (*53*). Thus, in both taxonomic composition and depositional age, the Shibantan Member represents an example of the Nama assemblage (*3*).

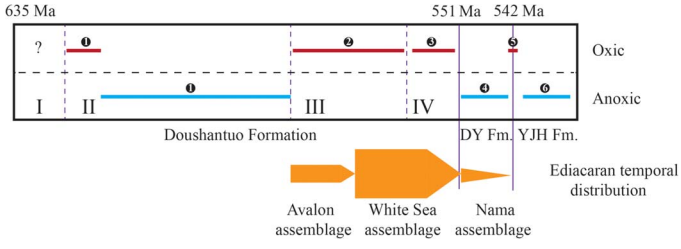

Fig. 4. Summary of global ocean redox chemistry in the Ediacaran and Early Cambrian periods. Data sources: 1, Fe-S-C systematics and redox-sensitive metal enrichments in euxinic shales from South China (*14*); 2, S and C isotopes in carbonates and siliciclastic rocks from Oman (*16*) and South China (*15*); 3, redox-sensitive metal enrichments and Mo-U isotopes in organic-rich shales from South China (*14*, *50*, *52*); 4, U isotopes in carbonates from South China (this study); 5, U isotopes in carbonates (this study), Mo isotopes in phosphorites (*49*), and redox-sensitive trace metal enrichments in euxinic shales from South China (*14*); 6, U isotopes in carbonates (this study). I to IV: Members I to IV of the Doushantuo Formation. The Ediacaran temporal distribution is modified after Laflamme *et al.* (*3*).

In the context of the dynamic redox model presented in this paper (Fig. 4), it is tempting to consider the potential correlation between ocean redox history and the evolution of the Ediacara biota. It seems that the Ediacara biota diversified and thrived as oxygenated conditions prevailed at 570 to 550 Ma ago but started to decline as oceanic anoxia began to expand globally around 550 Ma ago. Among the three assemblages of the Ediacara biota, the White Sea assemblage shows the peak diversity, and there is a significant decline in both global and local taxonomic diversity from the White Sea to the Nama assemblage (*2*–*5*). This decline in the terminal Ediacaran Period seems to be a robust pattern that has been supported by rarefaction analyses of both global and local taxonomic data (*4*, *5*). The U isotope data presented here suggest that oxic water masses began to contract around 550 Ma ago, raising the intriguing possibility that decline of the Ediacara biota is correlated with and may be caused by the expansion of oceanic anoxia and dynamic redox conditions in both temporal and spatial scales. It is possible that the terminal Ediacaran expansion of oceanic anoxia not only played a role in the decline of the Ediacara biota but also was a stimulus for the evolution of a new suite of mobile animals that could better explore localized oxygen oases or refugia (for example, oxic microenvironments associated with microbial mats). We emphasize that the possible role of anoxia in driving the decline of the Ediacara biota does not necessarily rule out the importance of ecological factors (*5*) because the environmental perturbation and biotic replacement models do not need to be mutually exclusive.

This study provides the first direct geochemical evidence supporting an episode of extensive oceanic anoxia in the terminal Ediacaran Period, coincident with the decline of the Ediacara biota as recorded in the Nama assemblage. Hence, the Ediacara biota likely capitalized on a geologically brief oxygenated window about 570 to 550 Ma ago, but subsequent oceanic anoxia along with other environmental and ecological factors may have contributed to its decline in the terminal Ediacaran Period.

METHODS

Analytical methods for uranium isotopes

Fresh carbonate samples that were collected from the field were crushed into small fragments in the laboratory. The fragments were cleaned using deionized water and dried. We carefully chose fresh fragments without veins and powdered these to <200 mesh using a ball mill and silicon nitride jars.

Approximately 3 g of each sample was dissolved in 1 M HCl at room temperature. This method minimizes dissolution of any noncarbonate minerals (for example, silicates and sulfides) and organic matter. Detailed protocols for the dissolution of ~3 g of carbonate powder are summarized in table S1. This protocol uses a 1.5× excess of HCl to ensure complete dissolution of the carbonate, thus avoiding U isotope fractionation from selective leaching of various carbonate phases.

Digests were left for 24 hours at room temperature to ensure complete reaction. Following this, samples were centrifuged, and the supernatant was separated. Major, minor, and trace element concentrations were measured on a Thermo iCAP quadrupole inductively coupled plasma mass spectrometer at the W. M. Keck Laboratory for Environmental Biogeochemistry at Arizona State University (ASU) on splits from each supernatant. Typical precision was better than 5% based on repeated analysis of in-run check standards.

Before column chemistry, appropriate amounts of the ^{236}U:^{233}U double spike (*19*, *23*, *29*) were added to each sample based on measured uranium concentrations. The spike-sample mixtures were evaporated to dryness and taken up in 3 N HNO_3. Uranium was purified using the UTEVA (Uranium and TEtraValent Actinides) method (*19*, *23*, *29*) for isotopic analysis. To minimize the matrix effects, all samples were put through column chemistry twice. Purified U was dissolved in 0.32 M HNO_3 and diluted to a U concentration of 50 parts per billion (ppb). Uranium isotopes were measured at ASU on a Thermo-Finnigan Neptune multi-collector ICP-MS at low mass resolution. When using a 75- and 100-μl min^{-1} nebulizer, a 50-ppb sample solution yielded 17 to 22 V and 38 to 45 V, respectively, of ^{238}U signal on a 10^{11}-ohm amplifier. Double spiked CRM145 (50 ppb of U) was analyzed by bracketing every group of two samples. A secondary standard (CRM129a) and an in-house ICP solution (Ricca PU1KN-100) were measured after every 15 measurements. Sample $\delta^{238}U$ values were normalized by the average of the bracketing standards.

The isotopic composition of standards CRM145, CRM129a, and Ricca was −0.00 ± 0.06‰ (2σ), −1.71 ± 0.05‰ (2σ), and −0.23 ± 0.06‰ (2σ), respectively, during the measurements of the Wuhe samples using a 100-μl min^{-1} nebulizer. The isotopic composition of standards CRM145, CRM129a, and Ricca was −0.00 ± 0.08‰ (2σ), −1.68 ± 0.08‰ (2σ), and −0.23 ± 0.08‰ (2σ), respectively, during the measurements of the Gaojiashan samples using a 75-μl min^{-1} nebulizer. The results (including samples, summary of standards, blanks, and sample replicates) are summarized in databases S1 to S4.

Analytical methods for carbon and oxygen isotopes of the Wuhe carbonate samples

Samples for $\delta^{13}C_{carb}$ and $\delta^{18}O$ were collected as ~300-g hand samples at 1-m intervals from a section near Wuhe, South China, and microdrilled using a 1-mm bit on a bench press drill following the procedures of Meyer *et al.* (*32*). Veins and vugs were avoided during drilling. The carbonate powders were then allowed to react with 100% phosphoric acid at 70°C in a MultiFlow-Geo headspace sampler device connected to an Isoprime 100 continuous flow isotope ratio mass spectrometer. Carbon and oxygen isotope compositions are reported in standard δ notation as per mil deviations from Vienna Pee Dee Belemnite. Reproducibility for repeated analysis of international standards IAEA-CO-1, IAEA-CO-9, and NBS 18 was better than 0.10‰ for $\delta^{13}C_{carb}$ and 0.22‰ for $\delta^{18}O_{carb}$.

SUPPLEMENTARY MATERIALS

Supplementary material for this article is available at http://advances.sciencemag.org/cgi/content/full/4/6/eaan8983/DC1

fig. S1. Simplified schematic representation of the major source and sinks of U in the modern ocean along with their isotopic compositions (sources) or associated isotopic fractionations (sinks) [modified after Tissot and Dauphas (*54*) and Wang *et al.* (*55*)].

fig. S2. Geochemical profiles for the study sections.

fig. S3. Petrographic images of the Hamajing Member.

fig. S4. Petrographic images of the Shibantan Member.

fig. S5. Petrographic images of the Baimatuo Member and the Yanjiahe Formation.

fig. S6. Chemostratigraphic profiles of $\delta^{238}U$, Sr content, Mn content, Mn/Sr ratio, and $\delta^{18}O$ for the study sections.

fig. S7. Chemostratigraphic profiles of $\delta^{238}U$, Mn/(Mg + Ca) ratio, and Sr/(Mg + Ca) ratio for the study sections.

fig. S8. Cross-plots of $\delta^{13}C$-$\delta^{18}O$ for the study sections.

fig. S9. Chemostratigraphic profiles of $\delta^{238}U$, Al content, Rb/Sr ratio, U/Al ratio, and Mg/Ca molar ratio for the study sections.

fig. S10. Chemostratigraphic profiles of U and Mo concentrations, Ce anomalies, U/(Mg + Ca) ratio, and Mo/(Mg + Ca) ratio for the study sections.

fig. S11. Mass balance modeling calculations show variations of seawater $\delta^{238}U$ values as a function of anoxic/euxinic seafloor area while keeping Δ_{anoxic} constant (+0.6‰) and testing various suboxic areal extents.
fig. S12. Calculated combination f_{anoxic} and $f_{suboxic}$ to account for latest Ediacaran seawater average $\delta^{238}U$ of −0.95‰.
table S1. The sample-dissolving procedure.
table S2. Cross-correlation coefficients (R^2) and P values calculated to test the influence of diagenetic indicators on $\delta^{238}U$ (confidence interval, 95%).
table S3. Summary of the parameters used in the modeling excise.
database S1. $\delta^{238}U$ data with associated geochemical data at the Wuhe section.
database S2. $\delta^{238}U$ data with associated geochemical data at the Gaojiashan section.
database S3. Analytical results of standard summary (Wuhe measurements).
database S4. Analytical results of standard summary (Wuhe measurements).
References (*54*–*100*)

REFERENCES AND NOTES

1. J. P. Pu, S. A. Bowring, J. Ramezani, P. Myrow, T. D. Raub, E. Landing, A. Mills, E. Hodgin, F. A. Macdonald, Dodging snowballs: Geochronology of the Gaskiers glaciation and the first appearance of the Ediacaran biota. *Geology* **44**, 955–958 (2016).
2. S. Xiao, M. Laflamme, On the eve of animal radiation: Phylogeny, ecology and evolution of the Ediacara biota. *Trends Ecol. Evol.* **24**, 31–40 (2009).
3. M. Laflamme, S. A. F. Darroch, S. M. Tweedt, K. J. Peterson, D. H. Erwin, The end of the Ediacara biota: Extinction, biotic replacement, or Cheshire Cat? *Gondwana Res.* **23**, 558–573 (2013).
4. B. Shen, L. Dong, S. Xiao, M. Kowalewski, The Avalon explosion: Evolution of Ediacara morphospace. *Science* **319**, 81–84 (2008).
5. S. A. F. Darroch, E. A. Sperling, T. H. Boag, R. A. Racicot, S. J. Mason, A. S. Morgan, S. Tweedt, P. Myrow, D. T. Johnston, D. H. Erwin, M. Laflamme, Biotic replacement and mass extinction of the Ediacara biota. *Proc. R. Soc. B* **282**, 20151003 (2015).
6. R. Tostevin, R. A. Wood, G. A. Shields, S. W. Poulton, R. Guilbaud, F. Bowyer, A. M. Penny, T. He, A. Curtis, K. H. Hoffmann, M. O. Clarkson, Low-oxygen waters limited habitable space for early animals. *Nat. Commun.* **7**, 12818 (2016).
7. S. Schröder, J. P. Grotzinger, Evidence for anoxia at the Ediacaran-Cambrian boundary: The record of redox-sensitive trace elements and rare earth elements in Oman. *J. Geol. Soc.* **164**, 175–187 (2007).
8. H. Kimura, Y. Watanabe, Oceanic anoxia at the Precambrian-Cambrian boundary. *Geology* **29**, 995–998 (2001).
9. J. E. Amthor, J. P. Grotzinger, S. Schröder, S. A. Bowring, J. Ramezani, M. W. Martin, A. Matter, Extinction of *Cloudina* and *Namacalathus* at the Precambrian-Cambrian boundary in Oman. *Geology* **31**, 431–434 (2003).
10. D. C. Catling, C. R. Glein, K. J. Zahnle, C. P. McKay, Why O_2 is required by complex life on habitable planets and the concept of planetary "oxygenation time". *Astrobiology* **5**, 415–438 (2005).
11. D. E. Canfield, S. W. Poulton, G. M. Narbonne, Late-Neoproterozoic deep-ocean oxygenation and the rise of animal life. *Science* **315**, 92–95 (2007).
12. N. J. Planavsky, C. T. Reinhard, X. Wang, D. Thomson, P. McGoldrick, R. H. Rainbird, T. Johnson, W. W. Fischer, T. W. Lyons, Earth history. Low Mid-Proterozoic atmospheric oxygen levels and the delayed rise of animals. *Science* **346**, 635–638 (2014).
13. R. A. Wood, S. W. Poulton, A. R. Prave, K.-H. Hoffmann, M. O. Clarkson, R. Guilbaud, J. W. Lyne, R. Tostevin, F. Bowyer, A. M. Penny, A. Curtis, S. A. Kasemann, Dynamic redox conditions control late Ediacaran metazoan ecosystems in the Nama Group, Namibia. *Precambrian Res.* **261**, 252–271 (2015).
14. S. K. Sahoo, N. J. Planavsky, G. Jiang, B. Kendall, J. D. Owens, X. Wang, X. Shi, A. D. Anbar, T. W. Lyons, Oceanic oxygenation events in the anoxic Ediacaran ocean. *Geobiology* **14**, 457–468 (2016).
15. K. A. McFadden, J. Huang, X. Chu, G. Jiang, A. J. Kaufman, C. Zhou, X. Yuan, S. Xiao, Pulsed oxidation and biological evolution in the Ediacaran Doushantuo Formation. *Proc. Natl. Acad. Sci. U.S.A.* **105**, 3197–3202 (2008).
16. D. A. Fike, J. P. Grotzinger, L. M. Pratt, R. E. Summons, Oxidation of the Ediacaran ocean. *Nature* **444**, 744–747 (2006).
17. S. Xiao, G. M. Narbonne, C. Zhou, M. Laflamme, D. V. Grazhdankin, M. Moczydlowska-Vidal, H. Cui, Towards an Ediacaran time scale: Problems, protocols, and prospects. *Episodes* **39**, 540–555 (2016).
18. E. A. Sperling, C. J. Wolock, A. S. Morgan, B. C. Gill, M. Kunzmann, G. P. Halverson, F. A. Macdonald, A. H. Knoll, D. T. Johnston, Statistical analysis of iron geochemical data suggests limited late Proterozoic oxygenation. *Nature* **523**, 451–454 (2015).
19. G. A. Brennecka, A. D. Herrmann, T. J. Algeo, A. D. Anbar, Rapid expansion of oceanic anoxia immediately before the end-Permian mass extinction. *Proc. Natl. Acad. Sci. U.S.A.* **108**, 17631–17634 (2011).
20. K. V. Lau, F. A. Macdonald, K. Maher, J. L. Payne, Uranium isotope evidence for temporary ocean oxygenation in the aftermath of the Sturtian Snowball Earth. *Earth Planet. Sci. Lett.* **458**, 282–292 (2017).
21. F. Zhang, T. J. Algeo, S. J. Romaniello, Y. Cui, L. Zhao, Z.-Q. Chen, A. D. Anbar, Congruent Permian-Triassic $\delta^{238}U$ records at Panthalassic and Tethyan sites: Confirmation of global-oceanic anoxia and validation of the U-isotope paleoredox proxy. *Geology* **46**, 327–330 (2018).
22. R. M. Dunk, R. A. Mills, W. J. Jenkins, A reevaluation of the oceanic uranium budget for the Holocene. *Chem. Geol.* **190**, 45–67 (2002).
23. S. Weyer, A. D. Anbar, A. Gerdes, G. W. Gordon, T. J. Algeo, E. A. Boyle, Natural fractionation of $^{238}U/^{235}U$. *Geochim. Cosmochim. Acta* **72**, 345–359 (2008).
24. M. B. Andersen, S. Romaniello, D. Vance, S. H. Little, R. Herdman, T. W. Lyons, A modern framework for the interpretation of $^{238}U/^{235}U$ in studies of ancient ocean redox. *Earth Planet. Sci. Lett.* **400**, 184–194 (2014).
25. E. A. Schauble, Role of nuclear volume in driving equilibrium stable isotope fractionation of mercury, thallium, and other very heavy elements. *Geochim. Cosmochim. Acta* **71**, 2170–2189 (2007).
26. M. Stylo, N. Neubert, Y. Wang, N. Monga, S. J. Romaniello, S. Weyer, R. Bernier-Latmani, Uranium isotopes fingerprint biotic reduction. *Proc. Natl. Acad. Sci. U.S.A.* **112**, 5619–5624 (2015).
27. A. Basu, R. A. Sanford, T. M. Johnson, C. C. Lundstrom, F. E. Löffler, Uranium isotopic fractionation factors during U(VI) reduction by bacterial isolates. *Geochim. Cosmochim. Acta* **136**, 100–113 (2014).
28. F. Zhang, S. J. Romaniello, T. J. Algeo, K. V. Lau, M. E. Clapham, S. Richoz, A. D. Herrmann, H. Smith, M. Horacek, A. D. Anbar, Multiple episodes of extensive marine anoxia linked to global warming and continental weathering following the latest Permian mass extinction. *Sci. Adv.* **4**, e1602921 (2018).
29. S. J. Romaniello, A. D. Herrmann, A. D. Anbar, Uranium concentrations and $^{238}U/^{235}U$ isotope ratios in modern carbonates from the Bahamas: Assessing a novel paleoredox proxy. *Chem. Geol.* **362**, 305–316 (2013).
30. D. Condon, M. Zhu, S. Bowring, W. Wang, A. Yang, Y. Jin, U-Pb ages from the neoproterozoic Doushantuo Formation, China. *Science* **308**, 95–98 (2005).
31. H. Cui, A. J. Kaufman, S. Xiao, S. Peek, H. Cao, X. Min, Y. Cai, Z. Siegel, X.-M. Liu, Y. Peng, J. D. Schiffbauer, A. J. Martin, Environmental context for the terminal Ediacaran biomineralization of animals. *Geobiology* **14**, 344–363 (2016).
32. M. Meyer, S. Xiao, B. C. Gill, J. D. Schiffbauer, Z. Chen, C. Zhou, X. Yuan, Interactions between Ediacaran animals and microbial mats: Insights from *Lamonte trevallis*, a new trace fossil from the Dengying Formation of South China. *Palaeogeogr. Palaeoclimatol. Palaeoecol.* **396**, 62–74 (2014).
33. Y. Cai, H. Hua, S. Xiao, J. D. Schiffbauer, P. Li, Biostratinomy of the late Ediacaran pyritized Gaojiashan Lagerstätte from southern Shaanxi, South China: Importance of event deposits. *Palaios* **25**, 487–506 (2010).
34. S. B. Jacobsen, A. J. Kaufman, The Sr, C and O isotopic evolution of Neoproterozoic seawater. *Chem. Geol.* **161**, 37–57 (1999).
35. Y. Sawaki, T. Ohno, M. Tahata, T. Komiya, T. Hirata, S. Maruyama, B. F. Windley, J. Han, D. Shu, Y. Li, The Ediacaran radiogenic Sr isotope excursion in the Doushantuo formation in the Three Gorges area, South China. *Precambrian Res.* **176**, 46–64 (2010).
36. A. S. Hood, N. J. Planavsky, M. W. Wallace, X. Wang, E. J. Bellefroid, B. Gueguen, D. B. Cole, Integrated geochemical-petrographic insights from component-selective $\delta^{238}U$ of Cryogenian marine carbonates. *Geology* **44**, 935–938 (2016).
37. G. Shields, J. Veizer, Precambrian marine carbonate isotope database: Version 1.1. *Geochem. Geophys. Geosyst.* **3**, 1–12 (2002).
38. D. E. Meece, L. K. Benninger, The coprecipitation of Pu and other radionuclides with $CaCO_3$. *Geochim. Cosmochim. Acta* **57**, 1447–1458 (1993).
39. X. Chen, S. J. Romaniello, A. D. Herrmann, L. E. Wasylenki, A. D. Anbar, Uranium isotope fractionation during coprecipitation with aragonite and calcite. *Geochim. Cosmochim. Acta* **188**, 189–207 (2016).
40. H.-F. Ling, X. Chen, D. Li, D. Wang, G. A. Shields-Zhou, M. Zhu, Cerium anomaly variations in Ediacaran–earliest Cambrian carbonates from the Yangtze Gorges area, South China: Implications for oxygenation of coeval shallow seawater. *Precambrian Res.* **225**, 110–127 (2013).
41. C. Holmden, M. Amini, R. Francois, Uranium isotope fractionation in Saanich Inlet: A modern analog study of a paleoredox tracer. *Geochim. Cosmochim. Acta* **153**, 202–215 (2015).
42. J. M. Rolison, C. H. Stirling, R. Middag, M. J. A. Rijkenberg, Uranium stable isotope fractionation in the Black Sea: Modern calibration of the $^{238}U/^{235}U$ paleo-redox proxy. *Geochim. Cosmochim. Acta* **203**, 69–88 (2017).
43. B. A. McKee, J. F. Todd, Uranium behavior in a permanently anoxic fjord: Microbial control? *Limnol. Oceanogr.* **38**, 408–414 (1993).
44. J. Bigeleisen, Nuclear size and shape effects in chemical reactions. Isotope chemistry of the heavy elements. *J. Am. Chem. Soc.* **118**, 3676–3680 (1996).

45. X. Wang, T. M. Johnson, C. C. Lundstrom, Isotope fractionation during oxidation of tetravalent uranium by dissolved oxygen. *Geochim. Cosmochim. Acta* **150**, 160–170 (2015).
46. S. Yang, B. Kendall, X. Lu, F. Zhang, W. Zheng, Uranium isotope compositions of mid-Proterozoic black shales: Evidence for an episode of increased ocean oxygenation at 1.36 Ga and evaluation of the effect of post-depositional hydrothermal fluid flow. *Precambrian Res.* **298**, 187–201 (2017).
47. C. Li, G. D. Love, T. W. Lyons, D. A. Fike, A. L. Sessions, X. Chu, A stratified redox model for the Ediacaran ocean. *Science* **328**, 80–83 (2010).
48. L. Xiang, S. D. Schoepfer, S.-. Shen, C.-. Cao, H. Zhang, Evolution of oceanic molybdenum and uranium reservoir size around the Ediacaran–Cambrian transition: Evidence from western Zhejiang, South China. *Earth Planet. Sci. Lett.* **464**, 84–94 (2017).
49. H. Wen, J. Carignan, Y. Zhang, H. Fan, C. Cloquet, S. Liu, Molybdenum isotopic records across the Precambrian-Cambrian boundary. *Geology* **39**, 775–778 (2011).
50. B. Kendall, T. Komiya, T. W. Lyons, S. M. Bates, G. W. Gordon, S. J. Romaniello, G. Jiang, R. A. Creaser, S. Xiao, K. McFadden, Y. Sawaki, M. Tahata, D. Shu, J. Han, Y. Li, X. Chu, A. D. Anbar, Uranium and molybdenum isotope evidence for an episode of widespread ocean oxygenation during the late Ediacaran Period. *Geochim. Cosmochim. Acta* **156**, 173–193 (2015).
51. T. M. Lenton, R. A. Boyle, S. W. Poulton, G. A. Shields-Zhou, N. J. Butterfield, Co-evolution of eukaryotes and ocean oxygenation in the Neoproterozoic era. *Nat. Geosci.* **7**, 257–265 (2014).
52. C. Scott, T. W. Lyons, A. Bekker, Y. Shen, S. W. Poulton, X. Chu, A. D. Anbar, Tracing the stepwise oxygenation of the Proterozoic ocean. *Nature* **452**, 456–459 (2008).
53. Z. Chen, C. Zhou, S. Xiao, W. Wang, C. Guan, H. Hua, X. Yuan, New Ediacara fossils preserved in marine limestone and their ecological implications. *Sci. Rep.* **4**, 4180 (2014).
54. F. L. H. Tissot, N. Dauphas, Uranium isotopic compositions of the crust and ocean: Age corrections, U budget and global extent of modern anoxia. *Geochim. Cosmochim. Acta* **167**, 113–143 (2015).
55. X. Wang, N. J. Planavsky, C. T. Reinhard, J. R. Hein, T. M. Johnson, A Cenozoic seawater redox record derived from $^{238}U/^{235}U$ in ferromanganese crusts. *Am. J. Sci.* **316**, 64–83 (2016).
56. T.-L. Ku, K. G. Knauss, G. G. Mathieu, Uranium in open ocean: Concentration and isotopic composition. *Deep Sea Res.* **24**, 1005–1017 (1977).
57. S. J. Romaniello, G. A. Brennecka, A. D. Anbar, A. S. Colman, Natural isotopic fractionation of $^{238}U/^{235}U$ in the water column of the Black Sea. *Eos Trans. AGU* **1**, 6(2009).
58. C. H. Stirling, M. B. Andersen, R. Warthmann, A. N. Halliday, Isotope fractionation of ^{238}U and ^{235}U during biologically-mediated uranium reduction. *Geochim. Cosmochim. Acta* **163**, 200–218 (2015).
59. M. B. Andersen, D. Vance, J. L. Morford, E. Bura-Nakić, S. F. M. Breitenbach, L. Och, Closing in on the marine $^{238}U/^{235}U$ budget. *Chem. Geol.* **420**, 11–22 (2016).
60. J. Noordmann, S. Weyer, R. B. Georg, S. Jöns, M. Sharma, $^{238}U/^{235}U$ isotope ratios of crustal material, rivers and products of hydrothermal alteration: New insights on the oceanic U isotope mass balance. *Isotopes Environ. Health Stud.* **52**, 141–163 (2016).
61. M. B. Andersen, C. H. Stirling, S. Weyer, Uranium isotope fractionation. *Rev. Mineral. Geochem.* **82**, 799–850 (2017).
62. J. L. Morford, S. Emerson, The geochemistry of redox sensitive trace metals in sediments. *Geochim. Cosmochim. Acta* **63**, 1735–1750 (1999).
63. M. B. Andersen, D. Vance, A. R. Keech, J. Rickli, G. Hudson, Estimating U fluxes in a high-latitude, boreal post-glacial setting using U-series isotopes in soils and rivers. *Chem. Geol.* **354**, 22–32 (2013).
64. A. Kaltenbach, "Uranium isotopic analysis of terrestrial and extraterrestrial samples," thesis, University of Otago (2013).
65. C. H. Stirling, M. B. Andersen, E.-K. Potter, A. N. Halliday, Low-temperature isotopic fractionation of uranium. *Earth Planet. Sci. Lett.* **264**, 208–225 (2007).
66. K. T. Goto, A. D. Anbar, G. W. Gordon, S. J. Romaniello, G. Shimoda, Y. Takaya, A. Tokumaru, T. Nozaki, K. Suzuki, S. Machida, T. Hanyu, A. Usui, Uranium isotope systematics of ferromanganese crusts in the Pacific Ocean: Implications for the marine $^{238}U/^{235}U$ isotope system. *Geochim. Cosmochim. Acta* **146**, 43–58 (2014).
67. G. A. Brennecka, L. E. Wasylenki, J. R. Bargar, S. Weyer, A. D. Anbar, Uranium isotope fractionation during adsorption to Mn-oxyhydroxides. *Environ. Sci. Technol.* **45**, 1370–1375 (2011).
68. Z. Chen, C. Zhou, M. Meyer, K. Xiang, J. D. Schiffbauer, X. Yuan, S. Xiao, Trace fossil evidence for Ediacaran bilaterian animals with complex behaviors. *Precambrian Res.* **224**, 690–701 (2013).
69. G. Jiang, X. Wang, X. Shi, S. Xiao, S. Zhang, J. Dong, The origin of decoupled carbonate and organic carbon isotope signatures in the early Cambrian (ca. 542–520 Ma) Yangtze platform. *Earth Planet. Sci. Lett.* **317–318**, 96–110 (2012).
70. G. Jiang, X. Shi, S. Zhang, Y. Wang, S. Xiao, Stratigraphy and paleogeography of the Ediacaran Doushantuo Formation (ca. 635–551 Ma) in South China. *Gondwana Res.* **19**, 831–849 (2011).
71. D. Chen, X. Zhou, Y. Fu, J. Wang, D. Yan, New U-Pb zircon ages of the Ediacaran-Cambrian boundary strata in South China. *Terra Nova* **27**, 62–68 (2015).
72. C. Zhou, S. Xiao, Ediacaran $\delta^{13}C$ chemostratigraphy of South China. *Chem. Geol.* **237**, 89–108 (2007).
73. G. J. Gilleaudeau, S. K. Sahoo, L. C. Kah, M. A. Henderson, A. J. Kaufman, Proterozoic carbonates of the Vindhyan Basin, India: Chemostratigraphy and diagenesis. *Gondwana Res.* **57**, 10–25 (2018).
74. J. L. Banner, G. N. Hanson, Calculation of simultaneous isotopic and trace element variations during water-rock interaction with applications to carbonate diagenesis. *Geochim. Cosmochim. Acta* **54**, 3123–3137 (1990).
75. G. J. Bowen, B. Wilkinson, Spatial distribution of $\delta^{18}O$ in meteoric precipitation. *Geology* **30**, 315–318 (2002).
76. L. C. Kah, J. K. Bartley, D. A. Teal, Chemostratigraphy of the Late Mesoproterozoic Atar Group, Taoudeni Basin, Mauritania: Muted isotopic variability, facies correlation, and global isotopic trends. *Precambrian Res.* **200–203**, 82–103 (2012).
77. L. C. Kah, A. G. Sherman, G. M. Narbonne, A. H. Knoll, A. J. Kaufman, $\delta^{13}C$ stratigraphy of the Proterozoic Bylot Supergroup, Baffin Island, Canada: Implications for regional lithostratigraphic correlations. *Can. J. Earth Sci.* **36**, 313–332 (1999).
78. A. J. Kaufman, A. H. Knoll, Neoproterozoic variations in the C-isotopic composition of seawater: Stratigraphic and biogeochemical implications. *Precambrian Res.* **73**, 27–49 (1995).
79. J. Veizer, Chemical diagenesis of carbonates: Theory and application of trace element technique, in *Stable Isotopes in Sedimentary Geology*, M. A. Arthur, T. F. Anderson, I. R. Kaplan, J. Veizer, L. S. Land, Eds. (Society of Economic Paleontologists and Mineralogists, Short Course Notes, 1983), vol. 10, pp. III-1–III-100.
80. V. C. Vahrenkamp, P. K. Swart, New distribution coefficient for the incorporation of strontium into dolomite and its implications for the formation of ancient dolomites. *Geology* **18**, 387–391 (1990).
81. S. J. Mazzullo, Geochemical and neomorphic alteration of dolomite: A review. *Carbonates Evaporites* **7**, 21–37 (1992).
82. J. D. Rimstidt, A. Balog, J. Webb, Distribution of trace elements between carbonate minerals and aqueous solutions. *Geochim. Cosmochim. Acta* **62**, 1851–1863 (1998).
83. A. S. Hood, M. W. Wallace, R. N. Drysdale, Neoproterozoic aragonite-dolomite seas? Widespread marine dolomite precipitation in Cryogenian reef complexes. *Geology* **39**, 871–874 (2011).
84. R. A. Wood, A. Y. Zhuravlev, S. S. Sukhov, M. Zhu, F. Zhao, Demise of Ediacaran dolomitic seas marks widespread biomineralization on the Siberian Platform. *Geology* **45**, 27–30 (2017).
85. R. L. Rudnick, S. Gao, Major elements of Earth Crust, in *Treatise on Geochemistry*, H. D. Holland, K. K. Turekian, Eds. (Elsevier, 2003), vol. 3, pp. 1–64.
86. R. Tostevin, G. A. Shields, G. M. Tarbuck, T. He, M. O. Clarkson, R. A. Wood, Effective use of cerium anomalies as a redox proxy in carbonate-dominated marine settings. *Chem. Geol.* **438**, 146–162 (2016).
87. S. J. Romaniello, A. D. Herrmann, A. D. Anbar, Syndepositional diagenetic control of molybdenum isotope variations in carbonate sediments from the Bahamas. *Chem. Geol.* **438**, 84–90 (2016).
88. K. V. Lau, K. Maher, D. Altiner, B. M. Kelley, L. R. Kump, D. J. Lehrmann, J. C. Silva-Tamayo, K. L. Weaver, M. Yu, J. L. Payne, Marine anoxia and delayed Earth system recovery after the end-Permian extinction. *Proc. Natl. Acad. Sci. U.S.A.* **113**, 2360–2365 (2016).
89. M. Elrick, V. Polyak, T. J. Algeo, S. Romaniello, Y. Asmerom, A. D. Herrmann, A. D. Anbar, L. Zhao, Z.-Q. Chen, Global-ocean redox variation during the middle-late Permian through Early Triassic based on uranium isotope and Th/U trends of marine carbonates. *Geology* **45**, 163–166 (2017).
90. C. Montoya-Pino, S. Weyer, A. D. Anbar, J. Pross, W. Oschmann, B. van de Schootbrugge, H. W. Arz, Global enhancement of ocean anoxia during oceanic anoxic event 2: A quantitative approach using U isotopes. *Geology* **38**, 315–318 (2010).
91. C. A. Partin, A. Bekker, N. J. Planavsky, C. T. Scott, B. C. Gill, C. Li, V. Podkovyrov, A. Maslov, K. O. Konhauser, S. V. Lalonde, G. D. Love, S. W. Poulton, T. W. Lyons, Large-scale fluctuations in Precambrian atmospheric and oceanic oxygen levels from the record of U in shales. *Earth Planet. Sci. Lett.* **369–370**, 284–293 (2013).
92. C. T. Reinhard, N. J. Planavsky, L. J. Robbins, C. A. Partin, B. C. Gill, S. V. Lalonde, A. Bekker, K. O. Konhauser, T. W. Lyons, Proterozoic ocean redox and biogeochemical stasis. *Proc. Natl. Acad. Sci. U.S.A.* **110**, 5357–5362 (2013).
93. N. Tribovillard, T. J. Algeo, T. Lyons, A. Riboulleau, Trace metals as paleoredox and paleoproductivity proxies: An update. *Chem. Geol.* **232**, 12–32 (2006).
94. C. E. Barnes, J. K. Cochran, Uranium removal in oceanic sediments and the oceanic U balance. *Earth Planet. Sci. Lett.* **97**, 94–101 (1990).
95. Y. Zheng, R. F. Anderson, A. van Geen, J. Kuwabara, Authigenic molybdenum formation in marine sediments: A link to pore water sulfide in the Santa Barbara Basin. *Geochim. Cosmochim. Acta* **64**, 4165–4178 (2000).
96. Y. Zheng, R. F. Anderson, A. van Geen, M. Q. Fleisher, Remobilization of authigenic uranium in marine sediments by bioturbation. *Geochim. Cosmochim. Acta* **66**, 1759–1772 (2002).

97. Y. Zheng, R. F. Anderson, A. van Geen, M. Q. Fleisher, Preservation of particulate non-lithogenic uranium in marine sediments. *Geochim. Cosmochim. Acta* **66**, 3085–3092 (2002).
98. J. H. Chen, R. Lawrence Edwards, G. J. Wasserburg, ^{238}U, ^{234}U and ^{232}Th in seawater. *Earth Planet. Sci. Lett.* **80**, 241–251 (1986).
99. D. W. Hastings, S. R. Emerson, A. C. Mix, Vanadium in foraminiferal calcite as a tracer for changes in the areal extent of reducing sediments. *Paleoceanography* **11**, 665–678 (1996).
100. H. H. Veeh, Deposition of uranium from the ocean. *Earth Planet. Sci. Lett.* **3**, 145–150 (1967).

Acknowledgments: We thank G. Gordon for her assistance with laboratory work at ASU and J. Wynn for sample preparation and laboratory assistance. **Funding:** We acknowledge funding from NASA Exobiology Program (no. NNX13AJ71G) and the NSF Frontiers in Earth System Dynamics program (award EAR-1338810). S.X. acknowledges support from a NASA grant (no. NNX15AL27G). B.K. acknowledges support from a Natural Sciences and Engineering Research Council of Canada Discovery Grant (RGPIN-435930). H.C. acknowledges funding from the American Association of Petroleum Geologists Grants-In-Aid Program and the Explorers Club Washington Group Exploration and Field Research Grant. M.M. acknowledges support from the Carnegie Institution for Science. **Author contributions:** F.Z., H.C., and A.D.A. designed the research; F.Z. performed the research and analyzed data; H.C., S.X., and M.M. provided samples and stratigraphic data. F.Z. and S.J.R. contributed to U isotope model calculations. S.X. and M.M. provided paleobiologic framework. All authors contributed with discussions. F.Z. wrote the manuscript with significant inputs from S.X., B.K., S.J.R., M.M., G.J.G., and A.D.A. **Competing interests:** The authors declare that they have no competing interests. **Data and materials availability:** All data needed to evaluate the conclusions in the paper are present in the paper and/or the Supplementary Materials. Additional data related to this paper may be requested from the authors.

Submitted 9 April 2017
Accepted 7 May 2018
Published 20 June 2018
10.1126/sciadv.aan8983

Citation: F. Zhang, S. Xiao, B. Kendall, S. J. Romaniello, H. Cui, M. Meyer, G. J. Gilleaudeau, A. J. Kaufman, A. D. Anbar, Extensive marine anoxia during the terminal Ediacaran Period. *Sci. Adv.* **4**, eaan8983 (2018).

Science Advances

Extensive marine anoxia during the terminal Ediacaran Period

Feifei Zhang, Shuhai Xiao, Brian Kendall, Stephen J. Romaniello, Huan Cui, Mike Meyer, Geoffrey J. Gilleaudeau, Alan J. Kaufman and Ariel D. Anbar

Sci Adv **4** (6), eaan8983.
DOI: 10.1126/sciadv.aan8983